European Polymer Journal 205 (2024) 112722

Contents lists available at ScienceDirect

European Polymer Journal

journal homepage: www.elsevier.com/locate/europolj

Exploring silk fibroin aerogels via different coagulation approaches

Martina Viola [a,b], Coraline Chartier [c], Marko Mihajlovic [a], Sijtze Buwalda [c], Christophe Pradille [d], Tatiana Budtova [c,*], Tina Vermonden [a,*]

[a] Department of Pharmaceutical Sciences (UIPS), Faculty of Science, Utrecht University, Utrecht, the Netherlands
[b] Department of Orthopaedics, University Medical Centre Utrecht, Utrecht, the Netherlands
[c] MINES Paris, PSL Research University, Centre for Materials Forming (CEMEF), UMR CNRS 7635, CS 10207, 06904 Sophia Antipolis, France
[d] Mat Xper, 19 Traverse du Barri, 06560, Sophia Antipolis, France

ARTICLE INFO

Keywords:
Bio-aerogels
Porosity
Mechanical properties
Coagulation of silk fibroin
Supercritical drying

ABSTRACT

Aerogels are highly porous nanostructured materials with a high specific surface area, a very low density and a low thermal conductivity. Bio-aerogels, prepared from biopolymers, have gained interest for biomedical applications. While most bio-aerogels are polysaccharide-based, protein-based aerogels using silk fibroin (SF) from *Bombyx mori* cocoons remain underexplored. Our study delved into the impact of coagulation methods on SF aerogel properties, specifically, comparing ethanol treatment (Method 1) and sodium dihydrogen phosphate (NaH_2PO_4) (Method 2). Aerogels obtained through Method 1 exhibited a volume shrinkage of approximately 12–22 % and a density of about 0.06–0.07 g cm^{-3}, while those obtained via Method 2 demonstrated a more substantial volume shrinkage of approximately 60–70 % and a higher density of around 0.2 g cm^{-3}. These differences significantly influenced the internal structure of the aerogels, manifesting distinct morphological features of the materials. Mechanical tests revealed that SF aerogels derived from Method 2 displayed superior stress resistance at 80 % strain and higher elastic recovery when compared to samples of Method 1. In conclusion, the choice in coagulation methods broadens the mechanical property and density window for this type of aerogel which offers opportunities for a wide range of biomedical applications.

1. Introduction

Bio-aerogels are biopolymer-based materials with a high porosity, high specific surface area, very low density and low thermal conductivity.[1,2] They are typically prepared by removing the pore liquid from a polymer network through drying with supercritical CO_2. Unlike ambient pressure drying, this method does not create capillary stresses in the pores, thereby theoretically preserving the porous, nanostructured network morphology of the starting gel. As a result of their dry nature, bio-aerogels retain their shape during long-term storage, and bacterial contamination can be avoided. Their unique physical characteristics make bio-aerogels appealing for a wide range of applications, including thermal insulation,[3] catalysis,[4] adsorption/absorption[5] and food-related applications.[6] In recent years, bio-aerogels have also been investigated for use as biomaterials,[7] for example as implantable biomedical devices,[8] tissue engineering scaffolds,[9] antibacterial materials[10] and drug delivery systems.[11].

Most bio-aerogels are based on polysaccharides because of their high availability and cost-effectiveness; for example, previously aerogels prepared from chitosan,[12] hyaluronic acid,[13] pectin[3] and cellulose[14] have been reported. Comparatively, bio-aerogels made from proteins are much scarcer, despite several advantageous features of proteins. Especially silk fibroin, which has been utilized in biomedicine for centuries as a material for suture threads, has gained increasing attention in the field of biomaterials thanks to its attractive properties including elasticity, biocompatibility and slow degradation *in vivo*.[15–17].

The most commonly used source of silk is from the *Bombyx mori* silkworm, which is readily available and affordable. *Bombyx mori* silk is composed of two main proteins: sericin and fibroin (SF). Sericin is a water-soluble protein that wraps around two parallel strands of SF. SF consists of two chains, one weighing approximately 26 kDa and the other around 390 kDa, connected by disulphide bonds.[18] To obtain pure SF, sericin, which is toxic to cells, is usually removed.[19] SF is a

* Corresponding authors at: Division of Pharmaceutics, Department of Pharmaceutical Sciences (UIPS), Faculty of Science, Utrecht University, Utrecht, the Netherlands (T. Vermonden).
E-mail addresses: tatiana.budtova@minesparis.psl.eu (T. Budtova), t.vermonden@uu.nl (T. Vermonden).

https://doi.org/10.1016/j.eurpolymj.2023.112722
Received 8 November 2023; Received in revised form 21 December 2023; Accepted 26 December 2023
Available online 28 December 2023

relatively hydrophobic protein primarily composed of glycine, alanine, serine, and tyrosine, making up about 99 % of its composition.[18] These peptidic strands can self-assemble to form strong and durable materials.[20] However, during the process of extracting SF, the protein's secondary structure is altered, resulting in a loss of elasticity and strength, which are typical characteristics of natural silk fibers.[20–22] To restore the secondary structure partially, various methods have been described in the literature, such as exposing the SF to ethanol, increasing the temperature, or using sonication. These methods promote the formation of β-sheets, which lead to a relatively brittle and weak material.[23,24] Our group has recently developed a different approach, inspired by the spider silk spinning process, using sodium dihydrogen phosphate (NaH_2PO_4) to coagulate SF.[25] This method induces self-assembly of the protein with fewer β-sheets compared to other coagulation techniques, while increasing the fraction of α-helices, resulting in a structure that is less crystalline and more elastic.

Only a limited amount of literature reported on SF aerogels. For example, Maleki *et al.* used a one-step or two-step sol–gel approach to prepare composite silica-SF aerogels for environmental applications and thermal insulation.[26,27] These composite aerogels exhibited lower thermal conductivity and higher compressibility and Young's modulus compared to neat silica aerogels. They were also shown to be printable using a micro-extrusion-based 3D printing approach.[28] Goimil *et al.* fabricated composite PCL aerogel scaffolds containing SF aerogel particles for bone tissue engineering.[29] The aerogel improved cell infiltration and biological fluid transport and allowed for modulation of the release kinetics of an anti-inflammatory drug. Another example involves SF aerogel fibers with incorporated noble metal nanoparticles for biological sensing and energy storage.[30] Mallepally et al. prepared neat SF hydrogels by using gaseous CO_2 as acidifying agent. Both CO_2 bubbling through a SF solution and the application of a high CO_2 pressure decreased the solution pH to the isoelectric point of SF (pH 4.0), resulting in gelation. The SF hydrogels were subsequently transformed into aerogels via supercritical CO_2 drying. The resulting aerogel scaffolds showed good cytocompatibility *in vitro* and have potential as materials for tissue engineering.[31,32].

Despite the information available in the existing reports on SF aerogels, as described above, little is known about the processing-structure-properties correlations. The purpose of the present work was to examine how the coagulation method of SF affects the structure and properties of the resulting aerogels. We compared SF aerogels obtained through two different coagulation methods, using either ethanol or NaH_2PO_4 treatment. While the former method has been extensively studied in previous research on SF materials, the latter was introduced in our recent work on electrowritten SF fibres, thereby yielding elastic materials.[25] We investigated the impact of the SF coagulation method and SF concentration on various characteristics of the resulting aerogels, such as volume shrinkage, density, specific surface area, morphology, and mechanical properties.

2. Materials and methods

2.1. Materials

Bombix mori cocoons were obtained from Evrosilk UK. Sodium carbonate (Na_2CO_3), polyethylene glycol (PEG, 6 kDa), cellulose dialysis tubes (MWCO 3.5 kDa), sodium dihydrogen phosphate (NaH_2PO_4) and ethanol (~99 %) were purchased from Sigma Aldrich. Lithium bromide (LiBr) was obtained from Acros Organics. Water was distilled.

2.2. Methods

2.2.1. SF extraction and dissolution

The SF was extracted from 20 g of *Bombix mori* cocoons as described by Kaplan et al.[19] Briefly, the cocoons were boiled in 8 L of water for 5 min. While the sericin protein dissolved in the water, the SF was precipitated as a fibrous solid. After rinsing SF with an excess of water and drying overnight at room temperature, SF (5.0 g) was dissolved in 20 mL of 9.3 M LiBr solution for 4 h. The SF solution was then dialyzed against distilled water for 4 days using cellulose dialysis tubes and concentrated using inverse dialysis against a PEG solution (30 % w/v) at 4 °C overnight using cellulose dialysis tubes. Solutions with SF concentrations of 10, and 15 % w/v in water were prepared. To check the SF concentration in solution, a known volume of aqueous SF solution, typically 50 mL, was weighed, dried at 60 °C for 1 h and dry weight measured.[19].

2.2.2. Aerogel preparation

Two methods were used to self-assemble/coagulate the protein in a network and make aerogels (Fig. 1): 1) The first was based on the addition of ethanol to a SF solution (Method 1). Ethanol leads to SF coagulation and formation of compact β-sheet structures.[33] 2) The second method (Method 2) involved the addition of an aqueous solution of 1 M sodium dihydrogen phosphate (NaH_2PO_4), which leads to structural rearrangement of protein from random coil to β-sheets and α-helices.[25].

In both cases, the process started with placing 1 mL of 10 % w/v or 15 % w/v SF aqueous solution in a cylindrical mold (1 cm in diameter) and gently adding 2 mL of either ethanol or NaH_2PO_4 solution on the SF solution surface, leading to coagulation of the protein solution resulting in formation of a 3D network (Fig. 1). To perform drying with supercritical CO_2 to make aerogels, the liquid in network pores should be miscible with CO_2. Samples treated with ethanol (Method 1) were subsequently washed in ethanol to remove excess of water (3 times per day for 4 days) resulting in "alcogel 1" and then dried with supercritical CO_2 resulting in "aerogel 1". Samples treated with NaH_2PO_4 (Method 2) were first washed with distilled water to remove the excess salt (by subsequent placing in 10 mL of water, three times) resulting in "hydrogel 2", then washed with ethanol (10 mL 3 times per day for 4 days) to remove the water resulting in "alcogel 2" and finally dried with supercritical CO_2 resulting in "aerogel 2".

Drying with supercritical CO_2 was performed as described elsewhere.[3,12,34] Briefly, the samples were placed in an autoclave under 50 bar and 37 °C, and ethanol was mixed with gaseous CO_2 (static mode). The pressure was then increased to 80 bar (above the critical value), to perform a dynamic washing step with an output of 5 kg h^{-1} of CO_2 for 1 h. These conditions were kept in the static mode of 1–2 h followed by a dynamic step for 2 h again. The system was then depressurized at 4 bar h^{-1}, cooled to room temperature and the samples were extracted.

Aerogels obtained with Method 1 are named SFX_EtOH and with Method 2 SFX_Na, where X corresponds to the SF concentration in the initial solution (10 or 15 % w/v).

2.2.3. Aerogels characterization

The volume of samples at each preparation step was measured using a caliper, and shrinkage in volume was calculated as follows:

$$Volume\ shrinkage\ (\%) = \frac{V_n - V_{n+1}}{V_n} \times 100\,\% \quad (1)$$

where V_n and V_{n+1} represent the volume before and after every step, respectively.

The bulk density ρ_{bulk} was calculated from the ratio of sample weight, measured with high-precision balance, and sample volume, measured with an Envelope Density Analyzer Geopyc 1360 (Micromeritics) with a calibrated chamber using DryFlo fine powder. Porosity and specific pore volume were calculated from bulk and skeletal density ($\rho_{skeletal} = 3.6\ g.cm^{-3}$)[28]:

$$Porosity\ (\%) = \frac{\rho_{skeletal} - \rho_{bulk}}{\rho_{skeletal}} \times 100\% \quad (2)$$

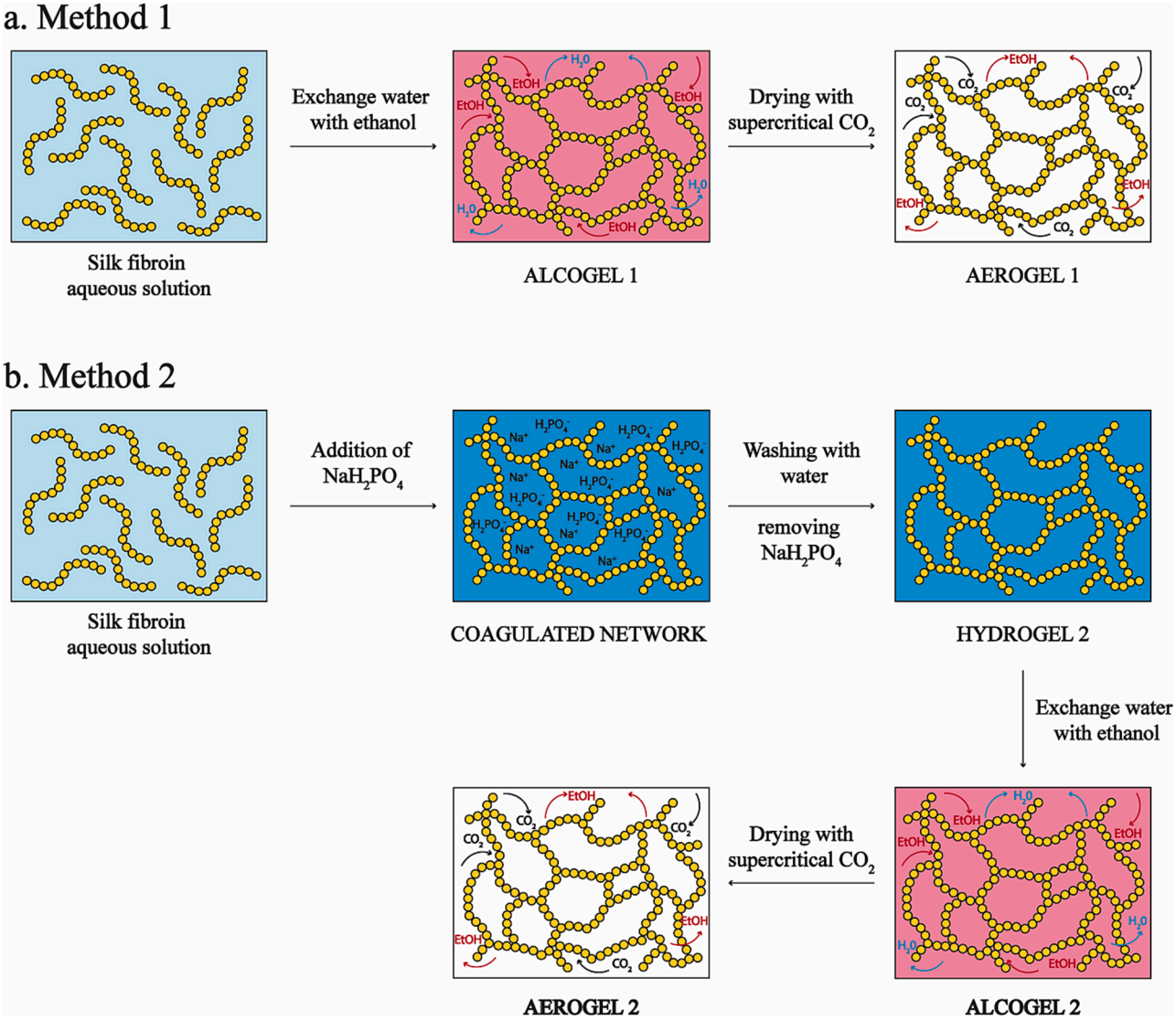

Fig. 1. Schematic presentation of two methods of SF aerogels preparation: Method 1 - via direct coagulation in ethanol and Method 2 - via coagulation in NaH_2PO_4.

$$Pore\ volume = \frac{1}{\rho_{bulk}} - \frac{1}{\rho_{skeletal}} \quad (3)$$

Specific surface area of aerogels was determined using an ASAP2020 Surface Area and Porosity Analyzer (Micromeritics) and the Brunauer, Emmett and Teller (BET) approach. Samples were degassed at 70 °C for 10 h.

The internal morphology of aerogels was studied with a Scanning Electron Microscope MAIA (Tescan) equipped with a field emission gun at an accelerating voltage of 3 keV. Samples were coated with a layer of platinum (14 nm) using a Q150T Quarum rotating metallizer.

The mechanical properties of SF aerogels were probed via uniaxial unconfined compression using an electromechanical testing machine Instron 5960 with a 30 kN load cell. Aerogels were made from 15 wt% SF solutions using Method 1 and Method 2. The samples were in the shape of cylinders of dimensions height/diameter around 17 mm/10 mm for aerogels made via Method 1 and 2 mm/10 mm for aerogels made via Method 2; the ratio height to diameter below 2 was used to avoid sample buckling and shear upon compression. The upper and lower surfaces of the cylinders were polished with P320 sandpaper to obtain parallel and planar surfaces. The sensor was calibrated in "class 0.5", which corresponds to less than 1 % error for the load 10 N-100 N and 0.5 % error for the load above 100 N. A preload of 1 N was applied to ensure the contact between machine plates and the sample. As samples were of different height, two different crosshead velocities, 1 mm min^{-1} for samples from Method 2 (SF_Na) and 5 mm/min for samples from Method 1 (SF_EtOH), were applied to ensure similar strain rates, (0.5 min^{-1} and 0.3 min^{-1}, respectively).

It is known that displacement measured by the testing machine is influenced by the stiffness of the machine itself, which leads to erroneous measurement of displacements. To correct for this, a Digital Image Correlation (DIC) approach was used. A speckle pattern using white and black paint was applied on the plates of the machine; this pattern allows direct tracking of the displacement which was recorded by two 5 MPX CCD Pike cameras (from AVT®) placed in stereo-correlation.

First, three cycles of loading/unloading at small strains, 5 %, 10 % and 15 %, were performed to test material elastic response (Fig. S1b). The compression was then continued up to 80 % of strain. As no sample broke, the relaxation after 80 % strain was recorded by maintaining the material in deformed state and measuring the evolution of stress over time. This test was used to determine the viscous term (or energy dissipation) of the material.

The compression experiments were analyzed using nominal stress σ_n vs nominal strain ε_n dependences (see Supporting Information, Fig. S1a):

$$\sigma_n = \frac{F}{A_0};\ \varepsilon_n = \frac{L - L_0}{L_0} \quad (4)$$

where F is force, A_0 is the cross-section area of the sample, and L_0 and L are the initial height of the sample and the height at a given applied force, respectively. Nominal values were used to compare with data known for mechanical properties of other bio-aerogels as true stress and true strain values have not been reported for bio-aerogels. The experiments were performed at room temperature and ambient pressure. At least 5 tests per formulation were performed.

2.3. Statistical analysis

All data are shown as mean ± SD, unless indicated otherwise. Statistical significance was tested by unpaired *t*-test with Welch's correction. All statistical analysis was performed with Prism 9 software (GraphPad).

3. Results and discussion

3.1. Visualization of SF aerogels, their properties and morphology

In the first step towards aerogel preparation, a non-solvent (ethanol or aqueous NaH_2PO_4) was added to SF solutions, inducing formation of a SF 3D network and change from transparent solutions to milky white samples (Fig. 2). This type of transformation is also commonly observed when polysaccharides undergo coagulation from a solution and form a network through non-solvent induced phase separation.[3,34,35].

The method used to make the 3D SF network has a significant impact on sample volume and the resulting network structure. When ethanol was used as non-solvent (Method 1), it rapidly diffused into the SF solution, resulting in alcogel 1 (Fig. 2a). Interestingly, the volume of this alcogel increased compared to the initial solution volume (Fig. 3a) resulting in a phenomenon called "negative shrinkage" or swelling. The swelling was 22 ± 17 % and 31 ± 10 % for 15 and 10 % SF concentration, respectively (Fig. 3c). This expansion occurred because the SF diffused into the liquid phase of ethanol, nearly filling the entire volume of the mold (Figure S2).

Subsequent drying with supercritical CO_2 caused some shrinkage of both alcogels (Fig. 3a, c for Method 1 and Fig. 3b, d for Method 2), as expected because of the lack of affinity of SF with non-polar CO_2, as also observed for numerous polysaccharide-based aerogels.[3,9,12,34,36] The total shrinkage of SF samples made using Method 1 was low, around 12 – 22 % (Fig. 3c).

When NaH_2PO_4 was used to form a SF network (Method 2), water was expelled from SF samples, resulting in significant volume shrinkage of approximately 60 – 70 % during the first step (see photos in Fig. 2, sample volume evolution for each step in Fig. 3b and volume shrinkage in Fig. 3d). Total shrinkage was around 70 – 80 % (Fig. 3b, d). We observed an uneven distribution of the material density in the sample, with the bottom part being denser than the top part where SF solution was in contact with NaH_2PO_4.

The average density of aerogels obtained with Method 1 was low, around 0.061 ± 0.003 g cm^{-3} for a SF concentration of 10 % in solution and 0.077 ± 0.004 g cm^{-3} for a SF concentration of 15 % (Fig. 3e). This is consistent with the density values typically seen for bio-aerogels made from polymer solutions of only a few percent. [3,9,12,34,36] In contrast, when Method 2 was used, the density was 0.248 ± 0.043 g cm^{-3} for a silk fibroin concentration of 10 % and 0.213 ± 0.021 g cm^{-3} for a SF concentration of 15 %, in correlation with the higher shrinkage observed for Method 2. It is noteworthy that there is an approximate 4 times difference in density between the aerogels obtained via the two methods. This disparity can be attributed to the different mechanisms of formation of SF networks. The difference between these two coagulation methods has been reported recently and can be explained by a higher amount of β-sheets in the SF coagulated with ethanol [23] compared to that coagulated with NaH_2PO_4. In the latter case, the number of α-helices is slightly higher. This difference is reflected in the mechanical properties of the final hydrogels.[25].

The surface area of SF aerogels made with both methods is around 230 – 330 m^2/g and within the experimental error does not depend on the method used nor on SF concentration (Fig. 3f). Similar values have been reported for aerogels made from chitosan, cellulose and starch. [10,35,37] Although coagulation of SF in NaH_2PO_4 induced rather high shrinkage, a certain mesoporosity was preserved.

3.2. Morphology of SF aerogels

The morphology of SF aerogels was investigated by analyzing SEM images, and representative examples of aerogels obtained with Method 1 and 2 are shown in Fig. 4. When comparing samples coagulated with the same method but from SF solutions of different concentrations, no significant difference was observed. However, a notable distinction was observed between the two coagulation methods. Both aerogels have a stable 3D skeleton structure, however SF_EtOH appeared with a typical highly porous net-like structure, while SF_Na appeared with a fibrous and intricate structure. One possible explanation for this can be linked to how the different coagulating agents interact with SF. In Method 1, ethanol mixes with the SF solution, diffuses between the polymer chains and coagulates the entire volume, thereby creating a porous net-like structure. In Method 2, on the other hand, phase separation immediately occurs upon contact with the NaH_2PO_4. Here, SF rapidly precipitates and sinks to the bottom in the form of fibrils, leading to the fibrous-beads structure. A similar morphology was reported for cellulose aerogels when cellulose was coagulated from solutions in ionic liquids.[37] However, in both aerogel types we observe inhomogeneity in the pore size distribution, which may be a consequence of the rudimental preparation method of the aerogel precursors (alcogel 1 and alcogel 2).

3.3. Mechanical properties of the aerogels

The mechanical properties of SF aerogels were evaluated under uniaxial compression (see Methods section). Fig. 5a and 5b show

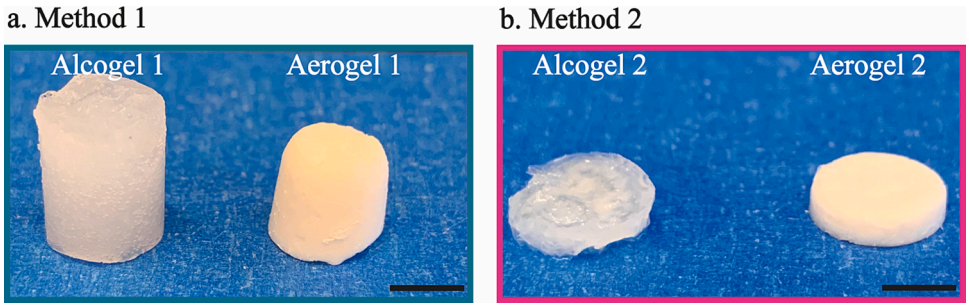

Fig. 2. Photos of SF alcogels and aerogels made from 15 %w/v SF solution using (a) Method 1 and (b) Method 2. The scale bar is 0.5 cm for all images.

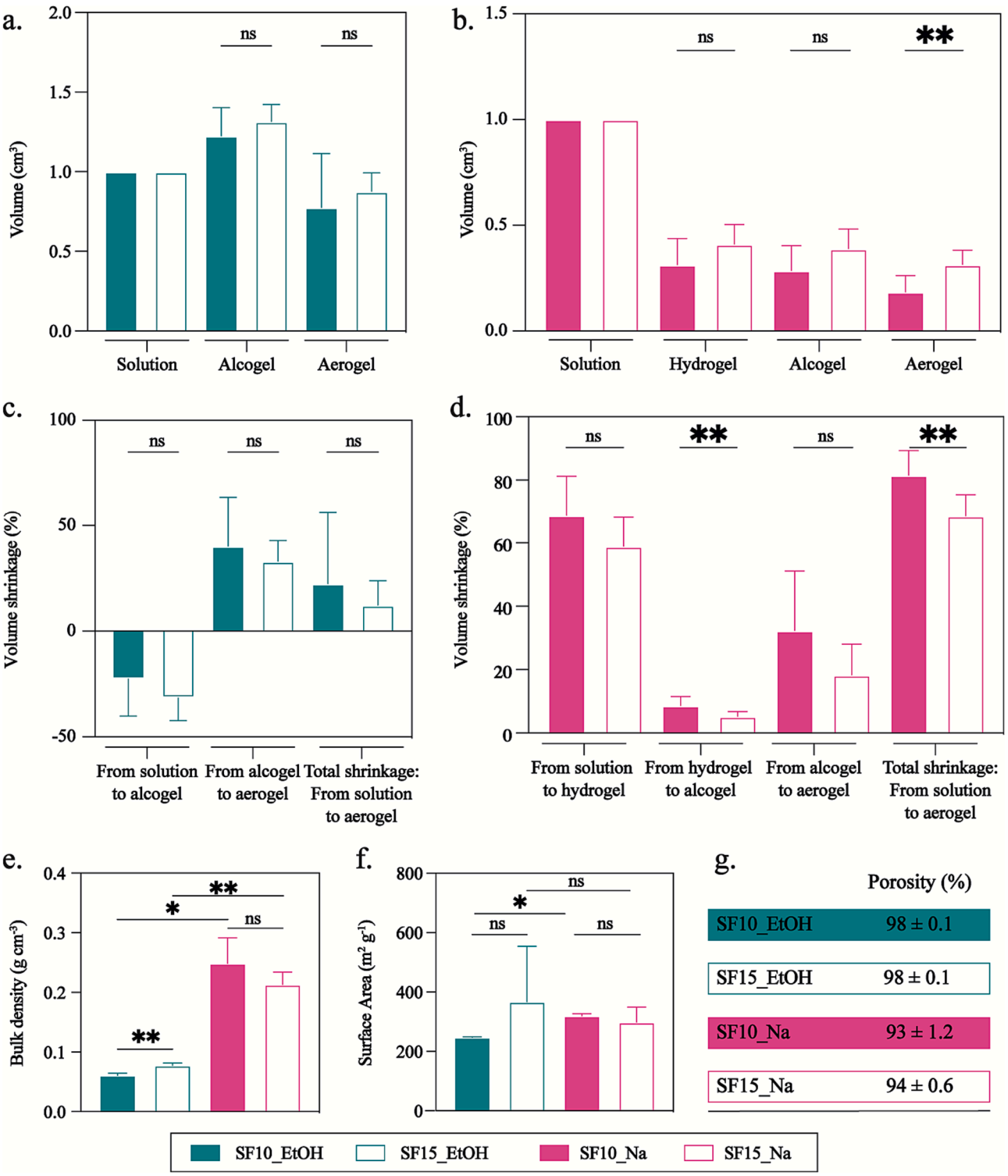

Fig. 3. Characteristics of all SF samples, (a, c) for Method 1 and (b, d) for Method 2:(a, b) Volume at every stage of the process, from solution to aerogel (** = $p < 0.01$); (c, d) shrinkage (* = $p < 0.05$; ** = $p < 0.01$); (e) density (* = $p < 0.05$, ** = $p < 0.01$, n = 3); (f) specific surface area (** = $p < 0.01$, n = 3); (g) porosity.

representative curves of the full stress–strain dependence and cycles at low strains for aerogels made with both methods, respectively (SF concentration in the initial solution was 15 %). None of the samples broke at any applied strain. The main characteristics, such as Young's modulus, elastic recovery and stress at 80 % strain, are presented in Fig. 5d.

The Young's moduli of the aerogels were determined within the elastic region, below 0.05 mm mm^{-1} strain, where an almost twofold increase is observed between SF15_EtOH and SF15_Na (Fig. 5d). Both values fall in the typical range of Young's moduli of bio-aerogels at the corresponding densities.[35] Lower values, of around 0.2 MPa and 0.09 MPa, were reported for a neat SF aerogel which can be explained by its lower density, of about 0.02 g cm^{-3}.[27,28] According to literature, it is known that Young's modulus tends to increase with density, and this is in agreement with what we have observed.[4,5,38].

The difference in aerogels' response to compression becomes more

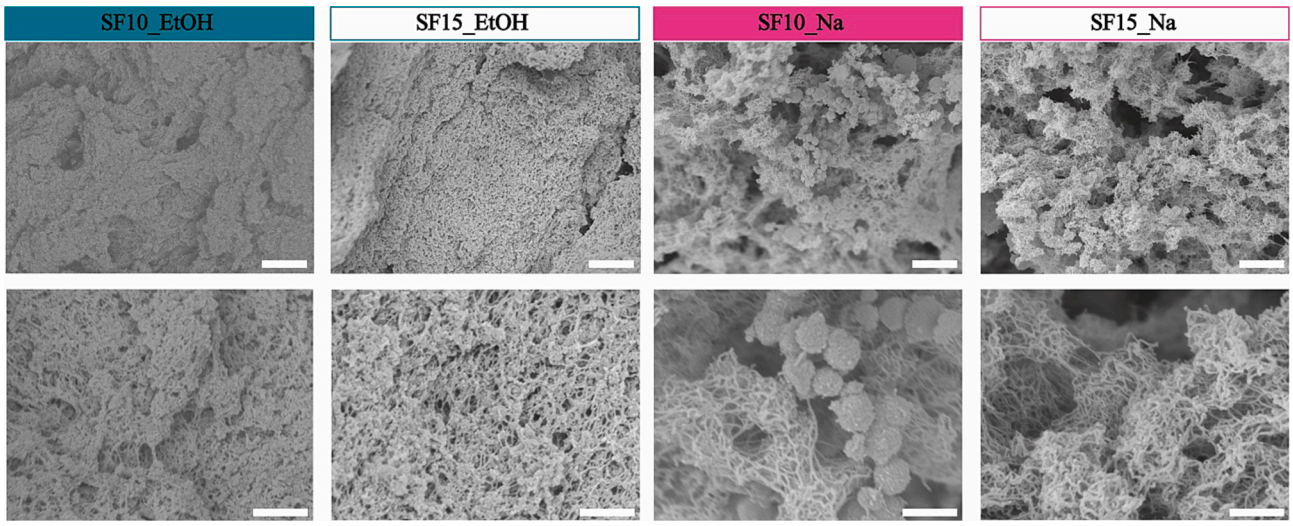

Fig. 4. SEM images of SF (10 and 15 %w/v) aerogels prepared after coagulation in ethanol or NaH_2PO_4 solution. Scale bar low magnification (top) 2 μm; scale bar high magnification (bottom) 500 nm.

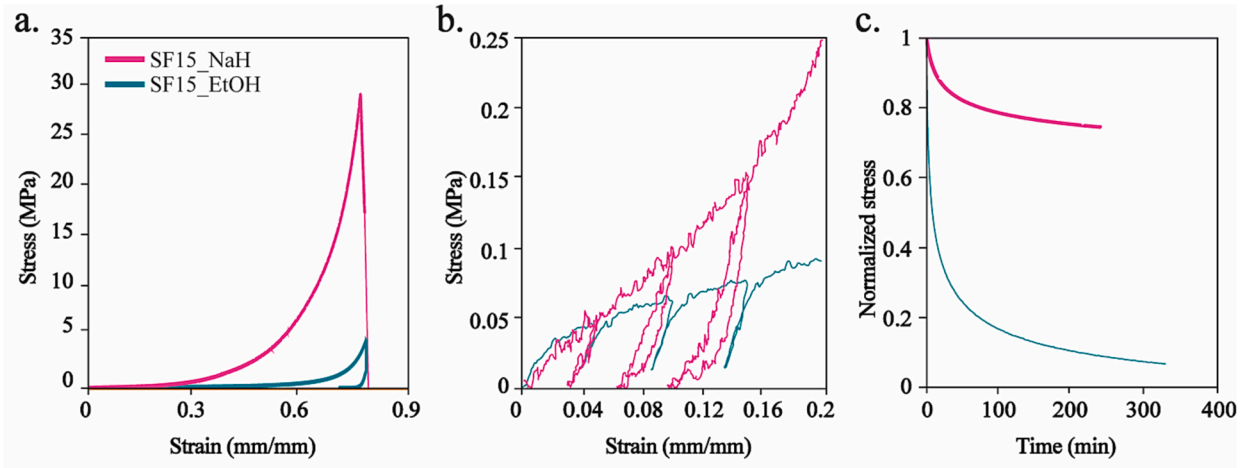

d.

	Density (g cm^{-3})	Young's Modulus (MPa)	Stress at 80% strain (MPa)	Elastic Recovery (%)	Relaxation after 250 sec (%)
SF15_EtOH	0.07 ± 0.02	0.8 ± 0.5	3.9 ± 0.8	1.0% ± 0.3%	71 ± 20
SF15_Na	0.20 ± 0.03	1.7± 0.5	31.0 ± 1.8	5% ± 1%	33 ± 10

Fig. 5. (a) Nominal stress–strain full curves and (b) at low strains for SF15_Na and SF15_EtOH aerogels; (c) Relaxation curves after stopping compression for SF15_Na and SF15_EtOH aerogels; (d) Main characteristics of SF aerogels: Young's modulus, stress at 80% strain, elastic recovery and relaxation after 250 s.

noticeable at strains above 0.05 mm mm^{-1}: for the same strain, an aerogel with higher density exhibits much higher stress. The stress recorded at 80 % strain is approximately eight times higher for the SF15_Na aerogel than for the SF15_EtOH aerogel (Fig. 5d). The maximal stresses obtained for both types of aerogels were 10 to 90 times higher than those of a SF aerogel reported in literature.[27,28].

The difference in the mechanical behavior of SF15_Na and SF15_EtOH aerogels was also observed in their response to cycles at low strains, which were performed to evaluate the elastic properties of the materials. The cycle allows deducing material elastic recovery, which was determined as the difference in strain at the upper and the lower point of the cycle. SF15_Na aerogels exhibited a larger stress hardening and higher elastic recovery, around 5 %, vs 1 % for SF15_EtOH aerogels. The shape of the cycle also provides information about the properties of the material: if the loading/unloading curves are superposed, the elastic term (in a visco-elastic solid) dominates the viscous term, as in the case of the SF15_EtOH aerogel.

Fig. 5c shows the response of SF aerogels after stopping compression and keeping the samples at 80 % strain. To compare the samples, the stress evolution over time after unloading was normalized to the corresponding values at 80 % strain. After 300 s the SF15_Na aerogel did not completely relax, reaching an asymptotic value of stress, while the residual stress in the SF15_EtOH aerogel reached almost zero. This behavior implies that SF15_Na aerogels maintain a level of stress and

structural integrity even after the removal of the compressive load, which can be advantageous in applications where long-term stability under sustained stress is critical.

4. Conclusions

In this study, we investigated the preparation of SF aerogels using two different coagulation methods: the traditional method using ethanol and an innovative, yet very simple method, using NaH_2PO_4. Our aim was to examine the impact of these coagulation methods on the morphological characteristics and mechanical properties of the aerogels. The results revealed significant differences between the aerogels produced with NaH_2PO_4 and those produced with ethanol. The volume shrinkage in the aerogel preparation step was higher for the samples coagulated with NaH_2PO_4, which can be attributed to the expulsion of water during coagulation, a phenomenon not observed in the ethanol coagulated samples. Aerogels coagulated with NaH_2PO_4 solution exhibited higher density and higher stiffness compared to those coagulated with ethanol, while maintaining the same surface area.

Furthermore, we observed significant differences in the internal structure of the two types of aerogels through SEM analysis. Aerogel 1 displayed a porous net-like structure, while aerogel 2 exhibited a fibrillar-beads structure. We can assert that the new method of silk fibroin coagulation using NaH_2PO_4 produces aerogels that exhibit higher density compared to those obtained through the traditional ethanol coagulation method. This leads to enhanced resistance to rupture when subjected to high compression loads.

These findings provide crucial insights regarding the effects of the coagulation method on the final material properties for the development of SF aerogels. Depending on the requirements of the application, a rational decision for the preparation method can now be selected, with the new NaH_2PO_4 treatment broadening the mechanical property and density window for this type of aerogel.

Silk fibroin (SF) aerogels, especially those coagulated with sodium dihydrogen phosphate (NaH_2PO_4), are promising for biomedical applications and drug delivery. Their high porosity and specific surface area could enhance biological fluid transport,[32] crucial for successful cell-material integration. Additionally, the porous nature could allow for drug incorporation, facilitate the diffusion and release of encapsulated drugs, an advantage in drug delivery systems requiring sustained therapeutic agent release.[39].

CRediT authorship contribution statement

Martina Viola: Writing – original draft, Conceptualization, Investigation, Methodology, Writing – original draft. **Coraline Chartier:** Conceptualization, Investigation, Methodology, Writing – original draft. **Marko Mihajlovic:** Conceptualization, Supervision, Writing – review & editing. **Sijtze Buwalda:** Conceptualization, Supervision, Writing – original draft, Writing – review & editing. **Christophe Pradille:** Methodology. **Tatiana Budtova:** Conceptualization, Funding acquisition, Supervision, Writing – review & editing. **Tina Vermonden:** Conceptualization, Funding acquisition, Supervision, Writing – review & editing.

Declaration of competing interest

The authors declare that they have no known competing financial interests or personal relationships that could have appeared to influence the work reported in this paper.

Data availability

Data will be made available on request.

Acknowledgments

The authors gratefully thank the following agencies for their financial support: PHC Van Gogh program (VGP.19/00010 and 44898RA 'AEROMED'), the Gravitation Program "Materials Driven Regeneration" (024.003.013) of the Dutch Research Council (NWO) and the Marie Skłodowska-Curie Actions (RESCUE #801540). We thank Dr. Julien Jaxel (PERSEE, Mines Paris) for drying samples with supercritical CO_2.

Data Availability: The data that support the findings of this study are available from the corresponding authors upon reasonable request.

Appendix A. Supplementary data

Supplementary data to this article can be found online at https://doi.org/10.1016/j.eurpolymj.2023.112722.

References

[1] T. Budtova, D.A. Aguilera, S. Beluns, L. Berglund, C. Chartier, E. Espinosa, S. Gaidukovs, A. Klimek-Kopyra, A. Kmita, D. Lachowicz, Biorefinery Approach for Aerogels, Polymers 12 (12) (2020) 2779.
[2] S. Zhao, W.J. Malfait, N. Guerrero-Alburquerque, M.M. Koebel, G. Nyström, Biopolymer aerogels and foams: Chemistry, properties, and applications, Angew. Chem. Int. Ed. 57 (26) (2018) 7580–7608.
[3] S. Groult, T. Budtova, Thermal conductivity/structure correlations in thermal super-insulating pectin aerogels, Carbohydr. Polym. 196 (2018) 73–81.
[4] Y. Tsutsumi, H. Koga, Z.-D. Qi, T. Saito, A. Isogai, Nanofibrillar chitin aerogels as renewable base catalysts, Biomacromolecules 15 (11) (2014) 4314–4319.
[5] Q. Ma, Y. Liu, Z. Dong, J. Wang, X. Hou, Hydrophobic and nanoporous chitosan–silica composite aerogels for oil absorption, J. Appl. Polym. Sci. 132 (15) (2015).
[6] L. Manzocco, F. Valoppi, S. Calligaris, F. Andreatta, S. Spilimbergo, M.C. Nicoli, Exploitation of κ-carrageenan aerogels as template for edible oleogel preparation, Food Hydrocoll. 71 (2017) 68–75.
[7] C.A. García-González, T. Budtova, L. Durães, C. Erkey, P. Del Gaudio, P. Gurikov, M. Koebel, F. Liebner, M. Neagu, I. Smirnova, An opinion paper on aerogels for biomedical and environmental applications, Molecules 24 (9) (2019) 1815.
[8] F. Sabri, M.E. Sebelik, R. Meacham, J.D. Boughter Jr, M.J. Challis, N. Leventis, In vivo ultrasonic detection of polyurea crosslinked silica aerogel implants, PLoS One 8 (6) (2013) e66348.
[9] M. Martins, A.A. Barros, S. Quraishi, P. Gurikov, S. Raman, I. Smirnova, A.R. C. Duarte, R.L. Reis, Preparation of macroporous alginate-based aerogels for biomedical applications, J. Supercrit. Fluids 106 (2015) 152–159.
[10] C. López-Iglesias, J. Barros, I. Ardao, P. Gurikov, F.J. Monteiro, I. Smirnova, C. Alvarez-Lorenzo, C.A. García-González, Jet cutting technique for the production of chitosan aerogel microparticles loaded with vancomycin, Polymers 12 (2) (2020) 273.
[11] S. Groult, S. Buwalda, T. Budtova, Tuning bio-aerogel properties for controlling drug delivery. Part 2: Cellulose-pectin composite aerogels, Biomaterials Advances 135 (2022) 212732.
[12] C. Chartier, S. Buwalda, H. Van Den Berghe, B. Nottelet, T. Budtova, Tuning the properties of porous chitosan: Aerogels and cryogels, Int. J. Biol. Macromol. 202 (2022) 215–223.
[13] L. Legay, T. Budtova, S. Buwalda, Hyaluronic Acid Aerogels Made Via Freeze–Thaw-Induced Gelation, Biomacromolecules 24 (2023) 4502–4509.
[14] L. Druel, A. Kenkel, V. Baudron, S. Buwalda, T. Budtova, Cellulose aerogel microparticles via emulsion-coagulation technique, Biomacromolecules 21 (5) (2020) 1824–1831.
[15] A.R. Murphy, D.L. Kaplan, Biomedical applications of chemically-modified silk fibroin, J. Mater. Chem. 19 (36) (2009) 6443–6450.
[16] A.R. Murphy, P.S. John, D.L. Kaplan, Modification of silk fibroin using diazonium coupling chemistry and the effects on hMSC proliferation and differentiation, Biomaterials 29 (19) (2008) 2829–2838.
[17] N. Gomez, C.E. Schmidt, Nerve growth factor-immobilized polypyrrole: Bioactive electrically conducting polymer for enhanced neurite extension, J. Biomed. Mater. Res. A 81 (1) (2007) 135–149.
[18] D.L. Kaplan, C. Vepari, Silk as a biomaterial, Prog Polym Sci 32 (2007) 991–1007.
[19] D.N. Rockwood, R.C. Preda, T. Yucel, X. Wang, M.L. Lovett, D.L. Kaplan, Materials fabrication from Bombyx Mori silk fibroin, Nat. Protoc. 6 (2011) 1612–1631.
[20] L.-D. Koh, Y. Cheng, C.-P. Teng, Y.-W. Khin, X.-J. Loh, S.-Y. Tee, M. Low, E. Ye, H.-D. Yu, Y.-W. Zhang, Structures, mechanical properties and applications of silk fibroin materials, Prog. Polym. Sci. 46 (2015) 86–110.
[21] L.S. Wray, X. Hu, J. Gallego, I. Georgakoudi, F.G. Omenetto, D. Schmidt, D. L. Kaplan, Effect of processing on silk-based biomaterials: Reproducibility and biocompatibility, J. Biomed. Mater. Res. B Appl. Biomater. 99 (1) (2011) 89–101.
[22] Q. Wang, S. Ling, Q. Yao, Q. Li, D. Hu, Q. Dai, D.A. Weitz, D.L. Kaplan, M. J. Buehler, Y. Zhang, Observations of 3 nm silk nanofibrils exfoliated from natural silkworm silk fibers, ACS Materials Letters 2 (2) (2020) 153–160.
[23] P. Monti, G. Freddi, A. Bertoluzza, N. Kasai, M. Tsukada, Raman spectroscopic studies of silk fibroin from Bombyx mori, J. Raman Spectrosc. 29 (4) (1998) 297–304.

[24] I. Chakraborty, K.J. Bodurtha, N.J. Heeder, M.P. Godfrin, A. Tripathi, R.H. Hurt, A. Shukla, A. Bose, Massive electrical conductivity enhancement of multilayer graphene/polystyrene composites using a nonconductive filler, ACS Appl. Mater. Interfaces 6 (19) (2014) 16472–16475.
[25] M. Viola, G. Cedillo-Servin, A.M. van Genderen, I. Imhof, M.P. Vena, M. Mihajlovic, S. Piluso, J. Malda, T. Vermonden, M. Castilho, Microstructured silk-fiber scaffolds with enhanced stretchability, bioRxiv 2023 (2023).
[26] H. Maleki, N. Huesing, Silica-silk fibroin hybrid (bio) aerogels: two-step versus one-step hybridization, J. Sol-Gel Sci. Technol. 98 (2021) 430–438.
[27] H. Maleki, L. Whitmore, N. Hüsing, Novel multifunctional polymethylsilsesquioxane–silk fibroin aerogel hybrids for environmental and thermal insulation applications, J. Mater. Chem. A 6 (26) (2018) 12598–12612.
[28] H. Maleki, S. Montes, N. Hayati-Roodbari, F. Putz, N. Huesing, Compressible, thermally insulating, and fire retardant aerogels through self-assembling silk fibroin biopolymers inside a silica structure—an approach towards 3D printing of aerogels, ACS Appl. Mater. Interfaces 10 (26) (2018) 22718–22730.
[29] L. Goimil, V. Santos-Rosales, A. Delgado, C. Evora, R. Reyes, A.A. Lozano-Perez, S. D. Aznar-Cervantes, J.L. Cenis, J.L. Gómez-Amoza, A. Concheiro, scCO_2-foamed silk fibroin aerogel/poly (ε-caprolactone) scaffolds containing dexamethasone for bone regeneration, J. CO2 Util. 31 (2019) 51–64.
[30] A.N. Mitropoulos, F.J. Burpo, C.K. Nguyen, E.A. Nagelli, M.Y. Ryu, J. Wang, R. K. Sims, K. Woronowicz, J.K. Wickiser, Noble metal composite porous silk fibroin aerogel fibers, Materials 12 (6) (2019) 894.
[31] R.R. Mallepally, M.A. Marin, M.A. McHugh, CO_2-assisted synthesis of silk fibroin hydrogels and aerogels, Acta Biomater. 10 (10) (2014) 4419–4424.
[32] R.R. Mallepally, M.A. Marin, V. Surampudi, B. Subia, R.R. Rao, S.C. Kundu, M. A. McHugh, Silk fibroin aerogels: Potential scaffolds for tissue engineering applications, Biomed. Mater. 10 (3) (2015) 035002.
[33] Y. Miyaguchi, J. Hu, Physicochemical properties of silk fibroin after solubilization using calcium chloride with or without ethanol, Food Sci. Technol. Res. 11 (1) (2005) 37–42.
[34] S. Groult, S. Buwalda, T. Budtova, Tuning bio-aerogel properties for controlling theophylline delivery. Part 1: Pectin aerogels, Mater. Sci. Eng. C 126 (2021) 112148.
[35] T. Budtova, Cellulose II aerogels: A review, Cellulose 26 (2019) 81–121.
[36] N. Buchtová, T. Budtova, Cellulose aero-, cryo-and xerogels: Towards understanding of morphology control, Cellulose 23 (2016) 2585–2595.
[37] F. Zou, T. Budtova, Tailoring the morphology and properties of starch aerogels and cryogels via starch source and process parameter, Carbohydr. Polym. 255 (2021) 117344.
[38] N. Buchtová, C. Pradille, J.-L. Bouvard, T. Budtova, Mechanical properties of cellulose aerogels and cryogels, Soft Matter 15 (39) (2019) 7901–7908.
[39] M.A. Marin, R.R. Mallepally, M.A. McHugh, Silk fibroin aerogels for drug delivery applications, J. Supercrit. Fluids 91 (2014) 84–89.